Deep learning reveals key aspects to help interpret the structure-property relationships of materials

Hieu-Chi Dam (dam@jaist.ac.jp)
Japan Advanced Institute of Science and Technology https://orcid.org/0000-0001-8252-7719
Tien-Sinh Vu
Japan Advanced Institute of Science and Technology
Minh-Quyet Ha
Japan Advanced Institute of Science and Technology
Duong Nguyen Nguyen
Japan Advanced Institute of Science and Technology
Viet-Cuong Nguyen
HPC SYSTEMS Inc.
Yukihiro Abe
HPC SYSTEMS Inc.
Truyen Tran
Deakin University
Huan Tran
Georgia Institute of Technology
Hiori Kino
National Institute for Materials Science https://orcid.org/0000-0002-8912-686X
Takashi Miyake
National Institute of Advanced Industrial Science and Technology https://orcid.org/0000-0003-2658-3470
Koji Tsuda
The University of Tokyo https://orcid.org/0000-0002-4288-1606

Article

Keywords: materials informatics, machine learning, neural network, attention model, structural representation

Posted Date: July 13th, 2023

DOI: https://doi.org/10.21203/rs.3.rs-3017049/v1

Additional Declarations: (Not answered)

Version of Record: A version of this preprint was published at npj Computational Materials on December 7th, 2023. See the published version at https://doi.org/10.1038/s41524-023-01163-9.

Deep learning reveals key aspects to help interpret the structure–property relationships of materials

Tien-Sinh Vu, Minh-Quyet Ha, Duong-Nguyen Nguyen, and Hieu-Chi Dam[a)]
Japan Advanced Institute of Science and Technology, 1-1 Asahidai, Nomi, Ishikawa 923-1292, Japan
Viet-Cuong Nguyen, Yukihiro Abe
HPC SYSTEMS Inc., 3-9-15 Kaigan, Minato, Tokyo 108-0022, Japan
Truyen Tran
Applied Artificial Intelligence Institute, Deakin University, Geelong, Australia
Huan Tran
School of Materials Science and Engineering, Georgia Institute of Technology, 771 Ferst Drive Northwest, Atlanta, Georgia 30332, United States
Hiori Kino
Research and Services Division of Materials Data and Integrated System, National Institute for Materials Science, 1-2-1 Sengen, Tsukuba, Ibaraki 305-0044, Japan
Takashi Miyake
Research Center for Computational Design of Advanced Functional Materials, National Institute of Advanced Industrial Science and Technology, 1-1-1 Umezono, Tsukuba, Ibaraki 305-8568, Japan
Koji Tsuda
Department of Computational Biology and Medical Sciences, Graduate School of Frontier Sciences, University of Tokyo, 5-1-5 Kashiwa-no-ha, Kashiwa-shi, Chiba-ken, 277-8561, Japan

(Dated: 6 June 2023)

Deep learning (DL) models currently used for materials research have limitations in providing meaningful information for interpreting predictions and understanding the relationships between structure and material properties. To address this, we propose a DL architecture that incorporates the attention mechanism to predict material properties and gain insights into their structure–property relationships. The proposed architecture is evaluated using four datasets: the QM9 molecule dataset and three in-house-developed computational materials datasets. Train–test–split validations confirm that the models derived from the proposed DL architecture exhibit strong predictive capabilities, comparable to those of current state-of-the-art models. Furthermore, comparative validations, based on first-principles calculations, indicate that the degree of attention of the atoms' local structures to the representation of the material structure is critical when interpreting structure–property relationships with respect to physical properties. The properties include molecular orbital energies or formation energies of crystals. Our proposed architecture shows great potential in accelerating material design by predicting material properties and identifying critical features of corresponding structures.

Keywords: materials informatics, machine learning, neural network, attention model, structural representation

I. Introduction

A central challenge in the field of materials science is using both experience and theory to explore the compositions and structures of materials with specific properties and subsequently validate them via experimentation. Unfortunately, the research and development of materials is a time-consuming endeavor that often relies on serendipity. To address these challenges, materials informatics (MI) has emerged as a rapidly growing interdisciplinary field that employs data-driven methods to extract practical knowledge regarding materials and their related physicochemical phenomena from experimental and computational data, thus ultimately accelerating the discovery of superior materials [1–4].

The majority of MI approaches consist of three key components[5]. The first component comprises datasets containing information regarding the structure of the materials, measurement results directly related to these structures, and physical properties relevant to the material development goals. The second component, i.e., representation, quantitatively describes the data instances in the first component, collecting a primitive description of materials for identification and analogical inference. The final component is a system that utilizes machine learning or data mining algorithms (either a single approach or a combination of approaches) to extract knowledge from the materials datasets for specific purposes, such as predicting properties or identifying new material compositions and structures.

Traditionally, materials are characterized by their elemental compositions and structures, and researchers rely

[a)]Electronic mail: dam@jaist.ac.jp

on their knowledge and experience (or tacit knowledge) to predict certain properties of hypothetical materials with a specific composition and structure. Computational chemistry approaches based on quantum mechanics, particularly density functional theory (DFT) simulations, can be used to theoretically verify the compositions and structures of these materials through $in-silico$ computational experimentation. However, computational experiments have limitations despite providing accurate information on the physical properties of hypothetical materials. For example, the vast number of potential hypothetical materials renders the design of materials with desired physical properties time-consuming and expensive due to the exhaustive calculations required. Moreover, researchers need specialized and detailed knowledge to narrow down the candidate compositions and material structures.

Unlike traditional approaches, MI approaches initially involve the conversion of primitive data descriptions into appropriate representations that can be used for mathematical reasoning and inference. In particular, MI systems are tasked with estimating qualitative and quantitative between materials based on these transformed representation, allowing them to uncover potential patterns in the material data[6–8]. The development of material representation (i.e., the design of material descriptors or methods for learning material representation from data) play a crucial role in MI approaches. This is because the effectiveness of an MI algorithm highly depends on the material representation, as it directly impacts the algorithm's performance and facilitates the explanation and interpretation of the inference process and prediction results[9]. Recent advancements in automated experiments and high-performance computers have enabled the acquisition of substantial experimental and computational data. Consequently, there is a growing need for the development of explainable and interpretable MI methods to enhance our understanding of physical and chemical phenomena.

Recently, various deep learning (DL)-based MI approaches have been developed to address challenges related to material representation and to predict physical properties[10–13]. A typical example is the DL architecture that uses a continuous-filter convolution layer with filter-generation networks to handle atomistic systems and accurately predict the properties of molecular and crystalline materials[10]. Another example is the convolutional neural network based on crystal graphs, which can predict material properties with an accuracy comparable to that of DFT calculations while also providing atomic-level chemical insight[12]. In addition to the aforementioned approaches, researchers have developed various other DL architectures to encode the local chemical environments of atoms and improve the prediction accuracy by integrating different types of material descriptors, applying graph neural networks (GNNs), and utilizing many-body tensor representations[11,13]. Furthermore, there are notable studies that incorporate prior knowledge to construct neural network models that ensure the properties of both outputs and inputs[14–16].

However, a significant challenge faced by both traditional and DL-based machine learning approaches is the issue interpretability. Machine learning models often prioritize including all available information rather than selecting an interpretable representation to improve prediction accuracy. The relationship between material representation and its properties is complex and nonlinear, resulting in machine learning models acting as "black boxes" that do not explicitly reveal correlations. Although statistical evaluations based on existing data often exhibit high prediction accuracies, estimating their predictive capability for new materials is challenging. Gaining detailed insight via machine learning to clarify underlying physicochemical phenomena also remains challenging.

Numerous studies have aimed to enhance model interpretability by incorporating additional information or features. For instance, graph convolutional networks use SMILES strings to represent molecules as inputs, enabling the identification of crucial fingerprint fragments and facilitating interpretation[17,18]. Despite this, these networks still require assistance in accurately predicting the properties of molecular and crystalline materials due to the absence of 3D structural information. Message-passing neural network-based models (MPNNs)[19–21] employ heuristic bonding information to capture atomic interactions but encounter difficulties with long-range interactions, feature interpretability, global information representation, and scalability when dealing with large molecule/crystal datasets. Attention-based models[16] are emerging as a potential solution to these limitations, offering superior parallel computational efficiency for large-scale applications. However, designing attention-based models specifically tailored for material structure representation is crucial for applications in materials science studies.

To address these challenges, we propose a DL architecture incorporating the attention mechanism to predict material structure properties and provide meaningful insights into these predictions. The proposed architecture starts by learning the representation of local structures of atoms within a material structure through the recursive application of attention mechanisms to the local structures of the neighboring atoms (Fig. 1a). The local structure of an atom includes the atom itself as the central atom, its neighboring atoms, and the arrangement of these atoms around the central atom. Finally, the material structure representation is derived from the representations of these local structures of the atoms. This architecture utilizes the attention mechanism to incorporate information about the geometrical arrangement of neighboring atoms into the representations of local structures. Moreover, it quantitatively measures the degree of attention given to each local structure from a global perspective when determining the representation of the material structure (Fig. 1b). Additionally, by training the

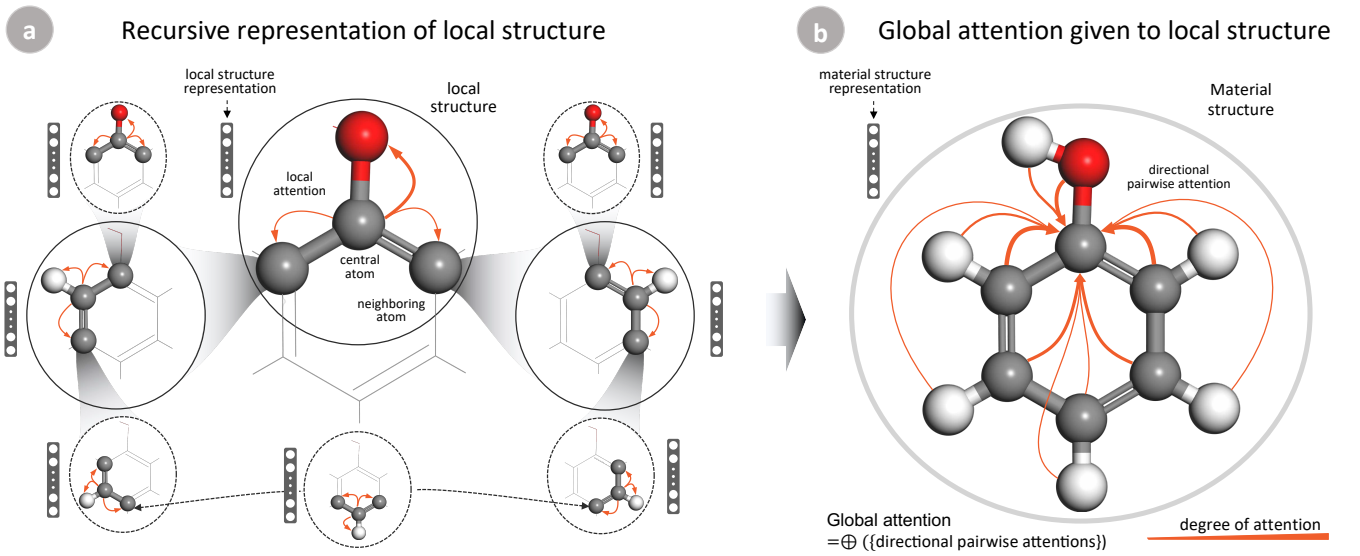

FIG. 1. Schematics of (a) the learning recursive representation of a local structure (central atom and its neighboring atoms) within the molecular structure of phenol (C_6H_5OH), and (b) measurement of the global attention given to a local structure when determining representation of the molecular structure. The direction and size of each arrow indicate the degree of attention given to other atoms when establishing the representation of the local structure of a particular atom.

model with specific target property, it becomes possible to determine the influence of information related to each atomic site on the final material structure representation with respect to the target property.

II. Results

A. SCANNet framework

We introduce a novel DL architecture called the Self-Consistent Attention Neural Network (SCANNet). SCANNet focuses on representing material structures from local structures of atoms with learned weights, thus facilitating the prediction and interpretation of material properties. The key objective of SCANNet is to recursively learn consistent representations of these local structures within the material (as shown in Fig. 1a), which are then appropriately combined to obtain an overall representation of the material structure.

In this study, each material structure S in a dataset $\mathcal{D}$ is represented using the atomic numbers and the corresponding coordinates of its M atoms. By employing Voronoi tessellation, a set of neighboring atoms $\mathcal{N}_i$ can be identified for each atom a_i in the structure S. Then, a vector $\mathbf{g}_{ij}$ is defined as the geometrical influence of a neighboring atom a_j on atom a_i ($1 \leq j \neq i \leq M$) (Section IV A). Next, SCANNet employs an embedding layer to express the atomic information of each atom a_i in S by an h-dimensional vector $\mathbf{c}_i^0$. Hereinafter, we denote the matrix $\mathbf{C}^0 = [\mathbf{c}_i^0]_{1\leq i\leq M}$ as $[\mathbf{c}_i^0]_{1\leq i\leq M} = [\mathbf{c}_1^0, \mathbf{c}_2^0, ..., \mathbf{c}_M^0]$. The SCANNet architecture consists of a series of L local attention layers and a global attention layer, each utilizing attention mechanisms[16] to represent the local structures within a material structure and the material structure itself, respectively. The layer-wise design of the local attention layers allows SCANNet to iteratively learn and improve the consistency of local structure representations, thereby providing information regarding long-range interactions between these local structures (Section IV B). For instance, the representation vector $\mathbf{c}_i^{l+1}$ of the local structure $\{a_i, \mathcal{N}_i\}$ at the $(l+1)^{th}$ local attention layer is derived as follows:

$$\mathbf{c}_i^{l+1} = \text{LocalAttention}^{l+1}(\mathbf{c}_i^l, \mathbf{C}_{\mathcal{N}_i}^l \times \mathbf{G}_{\mathcal{N}_i}), \qquad (1)$$

where $\mathbf{c}_i^l$ is the central atom at layer l^{th}, $\mathbf{C}_{\mathcal{N}_i}^l = [\mathbf{c}_j^l]_{a_j\in\mathcal{N}_i}$ denotes its neighboring local structures, and the geometrical influence of the neighboring atoms $\mathbf{G}_{\mathcal{N}_i} = [\mathbf{g}_{ij}]_{a_j\in\mathcal{N}_i}$.

The representation of a material structure is determined by linearly combining the representation vectors of its local structures, with global attention (GA) scores as the coefficients (Section IV C). Consequently, this approach can measure the amount of attention (GA scores) that should be given to a local structure by summing all corresponding directional pairwise attention scores from other local structures (Fig. 1b). We preserve the structural information of S from all representations of its local structures obtained at the final local attention layer to produce $\mathbf{C}^L$, where $\mathbf{C}^L = [\mathbf{c}_i^L]_{1\leq i\leq M}$. The global attention layer subsequently learns a suitable representation of the material structure based on the representations of its constituent local structures to accurately predict the material's properties.

$$\mathbf{x}_S = \text{GlobalAttention}(\mathbf{C}^L) = \sum_{i=1}^{M} \alpha_i^g \mathbf{k}_i^g, \qquad (2)$$

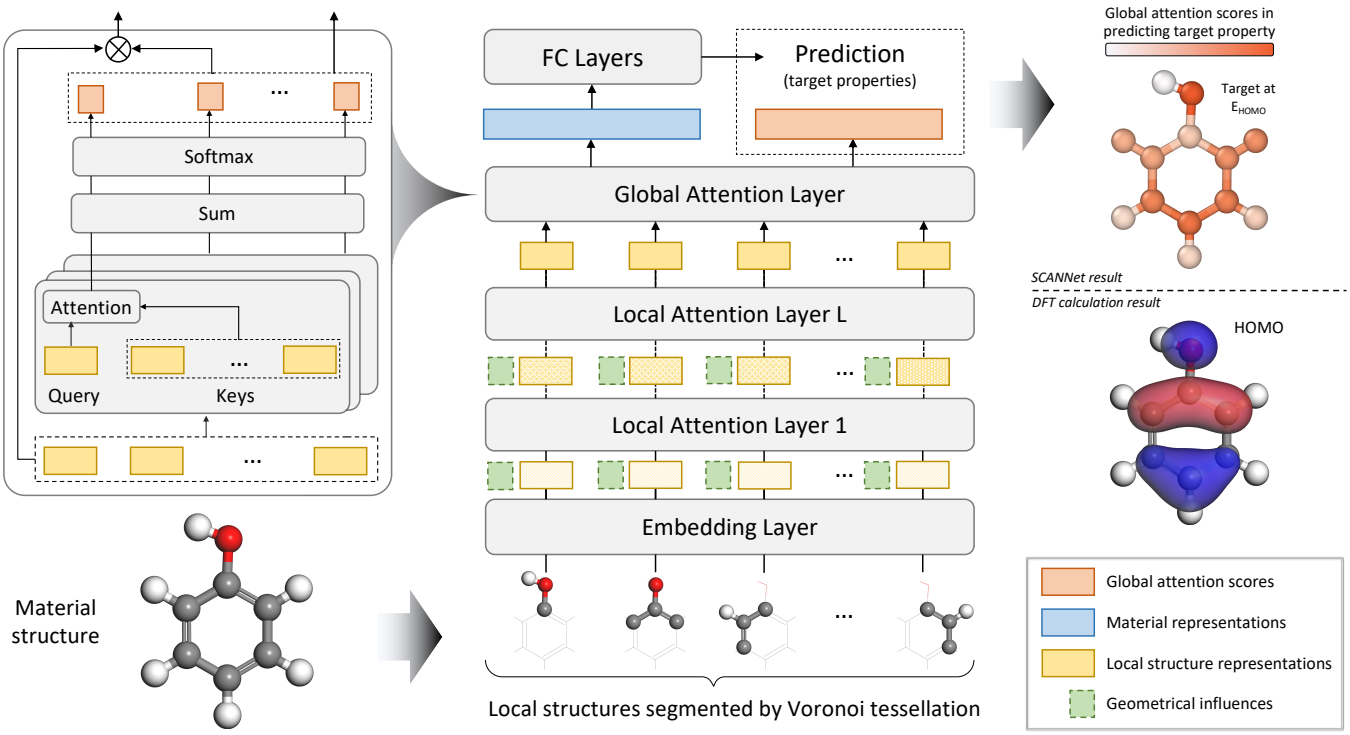

FIG. 2. Overview of the proposed SCANNet architecture, which is formed by stacking an embedding layer and local attention layers to learn the representations of various local structures in a material. In the readout stage, a global attention layer is used to assess the attention scores of these local structures. The attention score indicates the degree of attention that should be paid to a local structure to accurately represent the material and predict its physical property. The material representation is linearly combined based on the representations of its local structures with their corresponding attention scores. Fully connected (FC) layers are applied to the material representation to estimate the property of the material.

where $\mathbf{k}_i^g = \mathbf{c}_i^L \mathbf{W}_\mathbf{k}^g$ is the transformation of the local structure representation $\mathbf{c}_i^L$ and $\mathbf{W}_\mathbf{k}^g \in \mathbb{R}^{h\times h}$ is the learnable weight of the global attention layer. Consequently, the physical property y_S of the material structure S can be predicted from the learned representation $\mathbf{x}_S$ with fully connected layers F_S, as follows:

$$\hat{y}_S = F_S(\mathbf{x}_S), \tag{3}$$

Furthermore, the GA scores $\boldsymbol{\alpha}^g = [\alpha_1^g, \alpha_2^g, ..., \alpha_M^g]$ of the local structures, obtained from the global attention layer, help in identifying key factors that contribute to understanding the structure–property relationships of the material. A comprehensive depiction of the proposed SCANNet architecture is presented in Figure 2.

B. Experimental design

In this study, the proposed architecture's performance in predicting target properties and its ability to provide information regarding the structure–property relationship (interpretability) are evaluated using four molecular and crystal structure datasets (Table I). The properties of these datasets are determined through quantum mechanical calculations using DFT. The predictive capability is assessed by splitting the data into train-validation-test sets, where the models are trained on the training set and optimized based on the lowest mean absolute error (MAE) on the validation set. The MAEs of the predictions for the target properties on the test sets are reported for comparison with other models reported in the literature. Models fitted with parameters obtained using SCANNet are referred to as SCANNet models in

TABLE I. Summary of dataset information regarding seven properties analyzed with the SCANNet models, including dataset size (number of structures - #Size), number of atoms present in structures (#Atoms), and the specific physical properties examined.

Dataset	#Size	#Atoms	Properties
QM9[6]	130,831	4 to 29	$\mathbf{E}_{HOMO}$, $\mathbf{E}_{LUMO}$, $\mathbf{E}_{gap}$, α, C_v
Fullerence-MD[22]	3000	60, 70, 72	$\mathbf{E}_{HOMO}$, $\mathbf{E}_{LUMO}$
Pt/Graphene-MD[22]	21,666	103	ΔU
$SmFe_{12}$-CD[23]	3307	13	ΔE

$\mathbf{E}_{HOMO}$ (meV): Energy of the highest occupied molecular orbital; $\mathbf{E}_{LUMO}$ (meV): Energy of the lowest unoccupied molecular orbital; $\mathbf{E}_{gap}$ (meV): Energy gap; α ($bohr^3$): Isotropic polarizability; C_v (cal/mol K): Heat capacity at 298 K; ΔU (eV): Deformation energy; ΔE (eV/atom): Formation energy

this study. More details about the datasets used can be found in Section IV E.

Furthermore, the interpretability of the SCANNet models is assessed by examining the relationship between the learned GA scores of the local structures and the corresponding results from first-principles calculations. The results demonstrate the capability of the SCANNet models to provide valuable information regarding the structure–property relationships of materials in four scenarios: the local structures and HOMO/LUMO molecular orbitals (QM9[6] and Fullerene-MD[22]), the deformation energy ΔU and the deformation of the Pt/graphene structures (Pt/graphene-MD[22]), and the derived crystal formation energy and the substitution atom species and sites of $SmFe_{12}$-based compounds ($SmFe_{12}$-CD[23]).

C. Evaluation of the predictive power

Train–validation–test splits are performed in an 80:10:10 ratio to evaluate the predictive capability of SCANNet in predicting five physical material properties ($\mathbf{E}_{HOMO}$, $\mathbf{E}_{LUMO}$, $\mathbf{E}_{gap}$, α, and C_v) in the QM9 dataset. Five state-of-the-art DL methods with the MAE of the predictions derived from the models are also employed for comparison. The evaluation process is repeated five times to obtain an average MAE for the test set, thereby providing a robust assessment of the predictive capabilities of the models[14,15].

Table II presents the average MAE scores obtained from five training runs of the SCANNet models, as well as the corresponding scores for the competing models. In terms of $\mathbf{E}_{HOMO}$ prediction, the Cormorant model exhibited the best performance, with an MAE of 34 meV. The SCANNet model had an MAE of 41 meV for $\mathbf{E}_{HOMO}$ prediction, which is approximately 120% higher than the best model and 50% lower than the WaveScatt model. For the prediction of $\mathbf{E}_{LUMO}$, the MEGNet model exhibited the best performance, achieving the lowest MAE of 31 meV. Although the performance of the SCANNet model is not as good as those of the SE(3)-Trans and SchNet models, it is similar to that of the Cormorant model and significantly better than the WaveScatt model. Regarding $\mathbf{E}_{gap}$ prediction, the SE(3)-Trans model exhibited the best performance with an MAE of 53 meV. However, the results obtained using the SCANNet, Cormorant, MEGNet, and SchNet models are not significantly different, yielding values in the range of 61–63 meV. For α and C_v prediction, the Cormorant and MEGNet models outperform the other models significantly. Importantly, the performance of the proposed SCANNet model is comparable to that of the SE(3)-Trans model, with differences in MAE of less than 10% for these two target properties.

For the QM9 dataset, the widely accepted "chemical accuracy" thresholds are 43 meV for the three energy-related properties, $\mathbf{E}_{HOMO}$, $\mathbf{E}_{LUMO}$, and $\mathbf{E}_{gap}$; 0.1 $bohr^3$ for the isotropic polarizability α; and 0.05 $cal/molK$ for the heat capacity at 298 K[27]. Among the five properties, only the prediction error of the data-driven approaches for $\mathbf{E}_{gap}$ exceeds the threshold for chemical accuracy (i.e., 43 meV). However, for the remaining properties, at least two models achieved chemical accuracy. Notably, the SCANNet models demonstrated a prediction error of 41 meV for $\mathbf{E}_{HOMO}$, 37 meV for $\mathbf{E}_{LUMO}$ and 0.05 $cal/molK$ for C_v, indicating that chemical accuracy thresholds were achieved for these properties. To provide a more practical assessment of the models, considering real-world application scenarios and chemical accuracy thresholds, we evaluate the models by averaging their performance across the five target properties. Each property's evaluation is either the ratio of the prediction error to the chemical accuracy threshold (when the error exceeds the threshold) or 1 (when the error is below the threshold). The remarkable prediction accuracy of SCANNet confirms its practical applicability and guarantees that the interpretability derived from the attention scores effectively uncovers key structure–property relationships for the investigated material properties (Supplementary Table II).

TABLE II. Comparative evaluation of SCANNet and five other state-of-the-art DL models predicting five physical properties using the QM9 dataset. The bold numbers denote the lowest mean absolute errors (MAEs) among the six models.

	$\mathbf{E}_{HOMO}$ (meV)	$\mathbf{E}_{LUMO}$ (meV)	$\mathbf{E}_{gap}$ (meV)	α ($bohr^3$)	C_v (cal/mol K)
WaveScatt[24]	85	76	118	0.160	0.049
SchNet[25]	41	34	63	0.235	0.033
MEGNet[26]	38	**31**	61	**0.081**	0.030
Cormorant[14]	**34**	38	61	0.085	**0.026**
SE(3)-Trans[15]	35	33	**53**	0.142	0.054
SCANNet	41	37	61	0.141	0.050

$\mathbf{E}_{HOMO}$: Energy of the highest occupied molecular orbital; $\mathbf{E}_{LUMO}$: Energy of the lowest unoccupied molecular orbital; $\mathbf{E}_{gap}$: Energy gap; α: Isotropic polarizability; C_v: Heat capacity at 298 K.

The obtained results demonstrate that the SCANNet model achieves a prediction accuracy comparable to that of the five state-of-the-art DL methods and the "chemical accuracy" thresholds for predicting $\mathbf{E}_{HOMO}$, $\mathbf{E}_{LUMO}$, $\mathbf{E}_{gap}$, α, and C_v in the QM9 dataset. It is worth noting that SCANNet effectively learns representations of the molecular structures in the QM9 dataset solely based on the atoms' coordinates in the materials' structures. Incorporating conventional prior knowledge (e.g., atomic and bonding information between atoms, commonly utilized in message-passing neural network-based models) or adding physical constraints (e.g., equivalencies, covariates, and equations) into the learning process for material structure representations has the potential to enhance prediction accuracies. However, it is important to consider that these strategies can introduce biases

in the model by favoring certain materials, overlooking others, or oversimplifying complex phenomena, due to constraints or potential inaccuracies in the heuristic information assigned during the training phase. Consequently, such issues could hamper the clear understanding of structure-property relationships, which is the primary objective of this study.

Supplementary Section IV presents an evaluation of SCANNet's predictive capabilities on three in-house-developed material datasets, demonstrating its broad adaptability and high accuracy in diverse prediction scenarios.

D. Correspondence between the learned attentions of local structures and the molecular orbitals of small molecules:

For small molecules in the QM9 dataset, the SCANNet models demonstrate a remarkable correspondence between the obtained GA scores of the local structures and molecular orbitals results obtained by DFT calculations. As an example, Figure 3 shows comparisons between the GA scores of the local structures and the HOMO/LUMO orbitals obtained from DFT calculations for four molecules. Notably, an apparent correspondence between the relative GA scores of the local structures and the HOMO orbitals of the dimethyl butadiene molecule (*cis*-2,3-dimethyl-1,3-butadiene) is evident (Fig. 3a). Furthermore, the GA scores of the local structures can be easily linked to the interpretation that dimethyl butadiene readily undergoes the Diels–Alder reaction. Similarly, the correspondence between the HOMO orbital and the GA scores of the local structures is apparent for the thymine molecule (5-methyl pyrimidine-2,4 (1*H*,3*H*)-dione), one of the nucleobases in DNA (Fig. 3b).

Moreover, similar correspondences are confirmed between the GA scores of the local structures and the LUMO orbitals obtained from the DFT calculations for methyl acrylate (methyl prop-2-enoate) and dimethyl fumarate (dimethyl(2E)-but-2-enedioate). Methyl acrylate is a reagent commonly used in the synthesis of various pharmaceutical intermediates[28], whereas dimethyl fumarate has been proposed to exhibit immunomodulatory properties without causing significant immunosuppression[29]; thus, it has been evaluated as a potential treatment for COVID-19[30]. The apparent correspondence between the LUMO orbitals and the GA scores of the local structures of these two molecules (Fig. 3c and d) further highlight that the attention scores of the SCANNet model provide valuable insights for interpreting the structure–property relationships of molecules.

All carbon, nitrogen, and oxygen atomic sites in the QM9 dataset were statistically analyzed to systematically evaluate the GA scores obtained by the SCANNet models. Since the GA scores of atomic sites were normalized to 1, the relative GA scores were calculated based on the average GA score of the sp^3-hybridized carbon atoms in each molecule. Molecules without any sp3-hybridized carbon atoms were excluded (Fig. 4). The analysis of the GA scores for the HOMO energy reveals that the

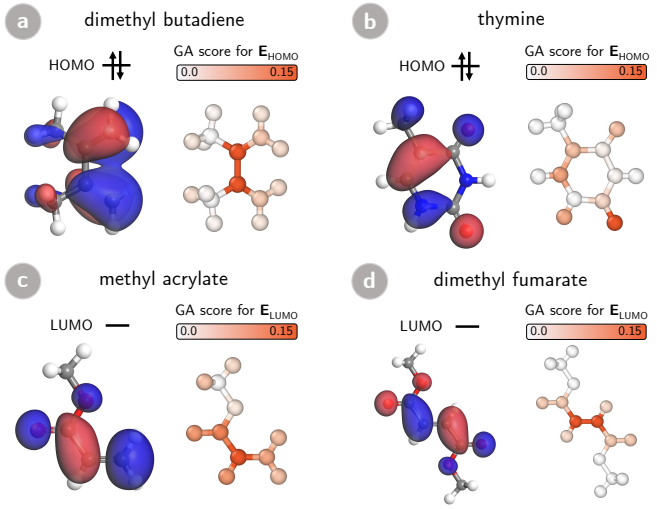

FIG. 3. Visualizations of structure–property relationships obtained from the SCANNet models for 4 molecules: (a) dimethyl butadiene, (b) thymine, (c) methyl acrylate, and (d) dimethyl fumarate. For each molecule, the left side of the figure illustrates the wave function of the HOMO (a), (b), or the LUMO (c), (d), as calculated by the DFT approach. The isosurfaces with positive and negative values of the wave functions are represented by blue and red lobes, respectively. The right-side figures display the GA scores of local structures derived from the SCANNet models for interpreting the corresponding molecular orbitals. The coloration of atoms and links between them do not signify the sign or nodes of the molecular orbital wave functions.

influence on HOMO follows the order of oxygen, nitrogen, and carbon. Specifically, sp^3-hybridized carbon sites have a lower influence compared to sp^2-hybridized or sp-hybridized carbon sites (Fig. 4a). These findings align with the electronegativity and bonding characteristics of the elements. Oxygen and nitrogen exhibit strong electronegativity and electron-rich regions in π-bonds, leading to a more significant electron density shift and higher HOMO energy localized around oxygen, nitrogen, and carbon sites with double or triple bonds.

In contrast, the GA scores for the LUMO energy show no significant difference between the three elements. This observation is consistent with the understanding that unoccupied orbitals primarily influence the LUMO, making the difference in electronegativity less pronounced compared to its effect on the HOMO energy (Fig. 4b).

E. Correspondence between the learned attentions of local structures and molecular orbitals of fullerene molecules:

To further evaluate the interpretability of the proposed method, the correspondence between the obtained GA scores of the local structures and the molecular orbitals obtained from DFT calculations for fullerene molecules is examined. Supplementary Figure 1 shows the GA scores of the local structures for the HOMO and LUMO energies of the C_{60} molecule (I_h symmetry). In this case,

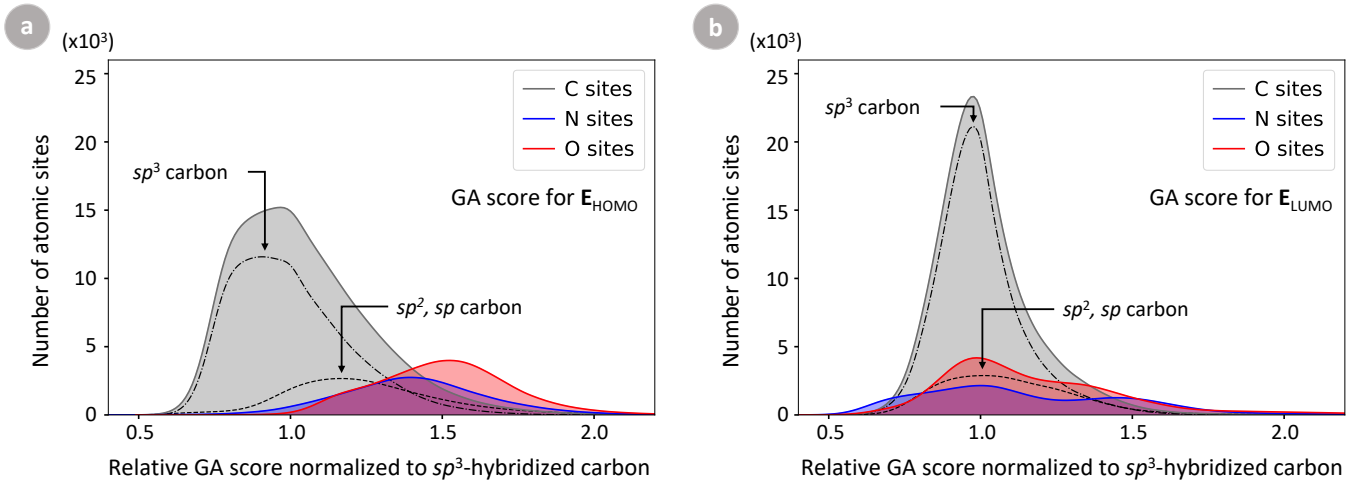

FIG. 4. Statistics of the relative GA scores for $\mathbf{E}_{HOMO}$ (a) and $\mathbf{E}_{LUMO}$ (b) for all carbon, nitrogen, and oxygen atomic sites in the molecular structures of the QM9 dataset, calculated based on the average GA score of sp^3-hybridized carbon atoms in each molecule. Gray, blue, and red lines and filled regions represent the statistics for carbon, nitrogen, and oxygen sites, respectively.

the target molecule has a truncated icosahedral structure composed of 20 hexagons and 12 pentagons, with all carbon atoms exhibiting equivalent local structures. The SCANNet model estimates identical GA scores for all local structures of the C_{60} molecule, thus indicating its ability to handle large and symmetric molecules.

As the number of carbon atoms in the fullerene molecule increases, the symmetry of the C_{70} (D_{5h} symmetry) and C_{72} (D_{6h} symmetry) molecules becomes slightly broken, and the local structures of the carbon atoms in these molecules are no longer equivalent. Figure 5 demonstrates a significant correspondence between the GA scores of the local structures and the HOMO and LUMO results obtained from DFT calculations for the C_{70} and C_{72} molecules. The GA scores of the local structures in the C_{70} and C_{72} molecules exhibit a five-fold (top view) and six-fold (top view) symmetry upon the prediction of the HOMO energy, respectively. These results align with the structural symmetry and degenerate HOMO orbitals of the two fullerene molecules. Notably, the C_{70} molecule possesses an additional 10-carbon ring, forming a plane symmetry, resulting in a planar symmetry of its HOMO with the node situated on that ring's plane. The SCANNet model reveals a clear correspondence between the HOMO of the C_{70} molecule and the GA scores of the local structures (Fig. 5a), as well as the LUMO and their corresponding GA scores. Furthermore, the shapes of LUMO and HOMO of the C_{72} molecule exhibit a perfect correspondence with the GA scores of the local structures obtained using the SCANNet models (Fig. 5b). Compared to C60, the C72 molecule has an additional ring of 24 carbon atoms with six-fold symmetry, consisting of 12 pairs of carbon–carbon bonds in five-membered carbon rings. The high GA scores of the local structures in the ring indicate the localization of the LUMO of the C_{72} molecule on the ring. In contrast, the HOMO orbitals are located on two opposite sides of the ring and are also captured by the local structures with high GA scores. This evaluation experiment provides further confirmation that SCANNet-derived GA scores offer valuable insights for understanding the structure–property relationship, even for large molecules.

F. Correspondence between the learned attentions of local structures and structural deformation in Pt/graphene:

Figure 6a presents the GA scores of the local structures obtained by the SCANNet model for predicting the deformation energy of a system comprising a platinum atom adsorbed on a graphene flake. The deformation energy is defined as the difference between the total energy of the deformed and optimized structures. A detailed examination of the obtained GA scores reveals that local structures with high GA scores possess relatively elongated carbon–carbon bonds (Fig. 6b). Additionally, the carbon atoms that form high local curvatures upon the formation of a convex from the planar structure of the sp^2 hybridization bonding network received high GA scores (Fig. 6c).

The results obtained from the experiment on the system where a platinum atom was adsorbed on a graphene flake reveal that the GA scores obtained by the SCANNet model exhibit a high correspondence with the observed structural deformations. In particular, the high GA scores for the increased carbon–carbon bond lengths and the convexed carbon atoms correspond well with the contribution to the deformation energy, as determined by DFT calculations. This finding indicates that the GA scores generated by SCANNet are reliable indicators of structural deformations in such systems, demonstrating the model's capability to capture and interpret the underlying material instability. These results validate the

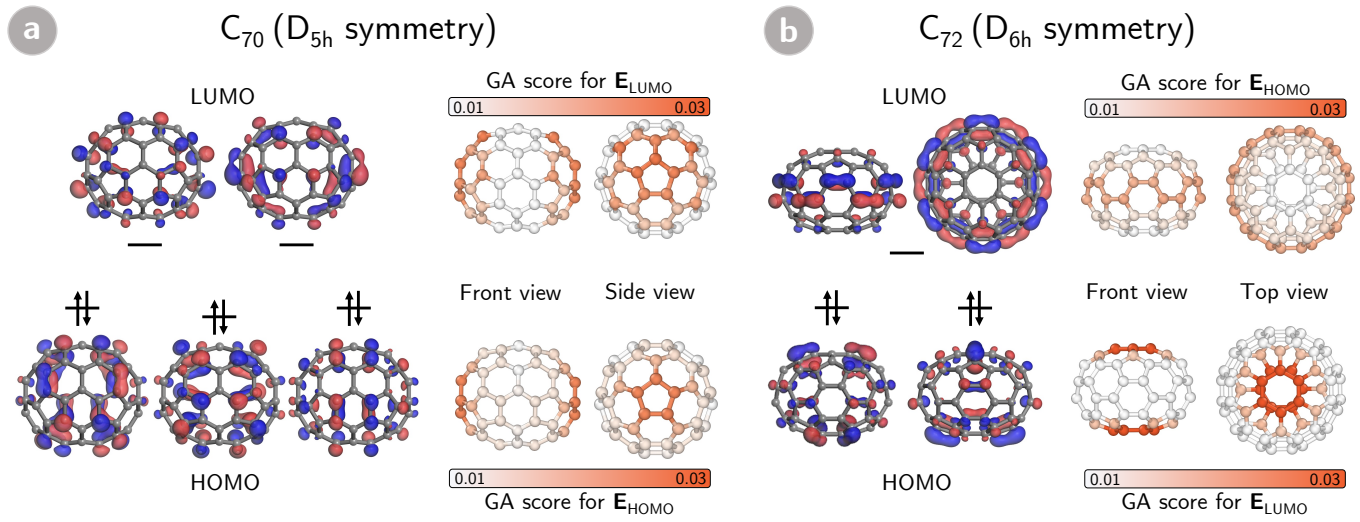

FIG. 5. Visualizations of structure–property relationships obtained from the SCANNet model for (a) C_{70} and (b) C_{72}. For each molecule, the left side of the figure illustrates the wave functions of the degenerate HOMO (bottom) and LUMO (top) orbitals, as calculated by the DFT approach. The isosurfaces with positive and negative values of the wave functions are represented by the blue and red lobes, respectively. The figure on the right displays the GA scores of local structures obtained using the SCANNet model for the corresponding property.

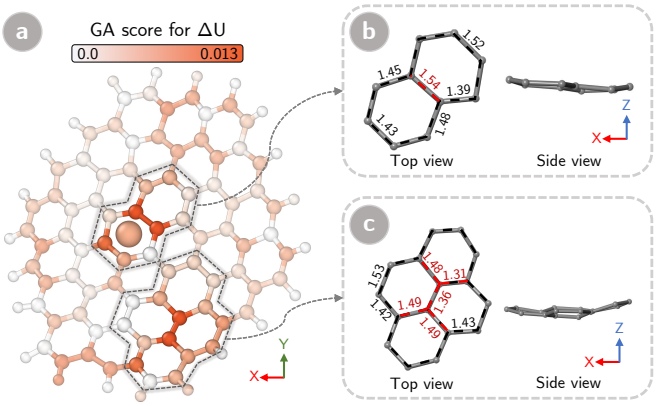

FIG. 6. Visualization of the relationship between the adsorption energy and the deformation of a graphene flake with a platinum atom adsorbed on a graphene flake. (a) Visualization of the GA scores obtained from the SCANNet model for the Pt/Graphene system with a deformation. Structural visualizations of the high attention local structures during the deformation: (b) elongated carbon–carbon bond, and (c) convexed carbon–carbon configuration. The distance from the carbon atom to the adjacent carbon atom (in Å) is highlighted to show the distortion caused by the deformation.

usefulness of SCANNet in understanding and predicting structural deformations in materials, particularly in cases involving the interaction of different elements or adsorption onto surfaces.

G. Correspondence between the learned attentions of local structures and stability of $SmFe_{12}$-based crystal structures:

The SCANNet model's ability to predict the formation energy of $SmFe_{12}$-based crystal structures is evaluated by analyzing the GA scores of atomic sites. The focus is on understanding the effects of substituting Fe sites with other elements on the derived formation energy and the stabilization of the crystal structure, as well as the influence of the elemental substitution on the formation energies of other Sm and Fe sites. Note that the GA scores of the local structures are normalized to ensure that the sum of the attention scores of all local structures in the crystal structure is equal to one.

For instance, Figure 7a shows the GA scores of the local structures obtained by the SCANNet model for predicting the formation energies of the $SmFe_{12}$, $SmFe_{11}Mo$, $SmFe_{11}Co$, and $SmFe_{11}Al$ crystal structures. For the optimized $SmFe_{12}$ crystal structure, all Fe sites receive identical GA scores, indicating a symmetric cage of Fe atoms surrounding the Sm atoms. Additionally, the negligible difference in GA scores between the Sm and Fe sites suggests that when analyzing the formation energy of the $SmFe_{12}$ crystal structure, greater attention should be given to the Fe sites rather than the Sm sites. This implies that Sm atoms are comfortably placed within the cage of Fe atoms in the SmFe12 crystal structure.

For the crystal structures with Mo substitutions, the GA scores of the Mo and Sm sites are estimated to be the same as those of the Fe sites. However, for crystal structures with Co or Al substitutions, the GA scores of the Co and Al sites are significantly higher than those of Fe sites. The GA score results for the three crystal structures in-

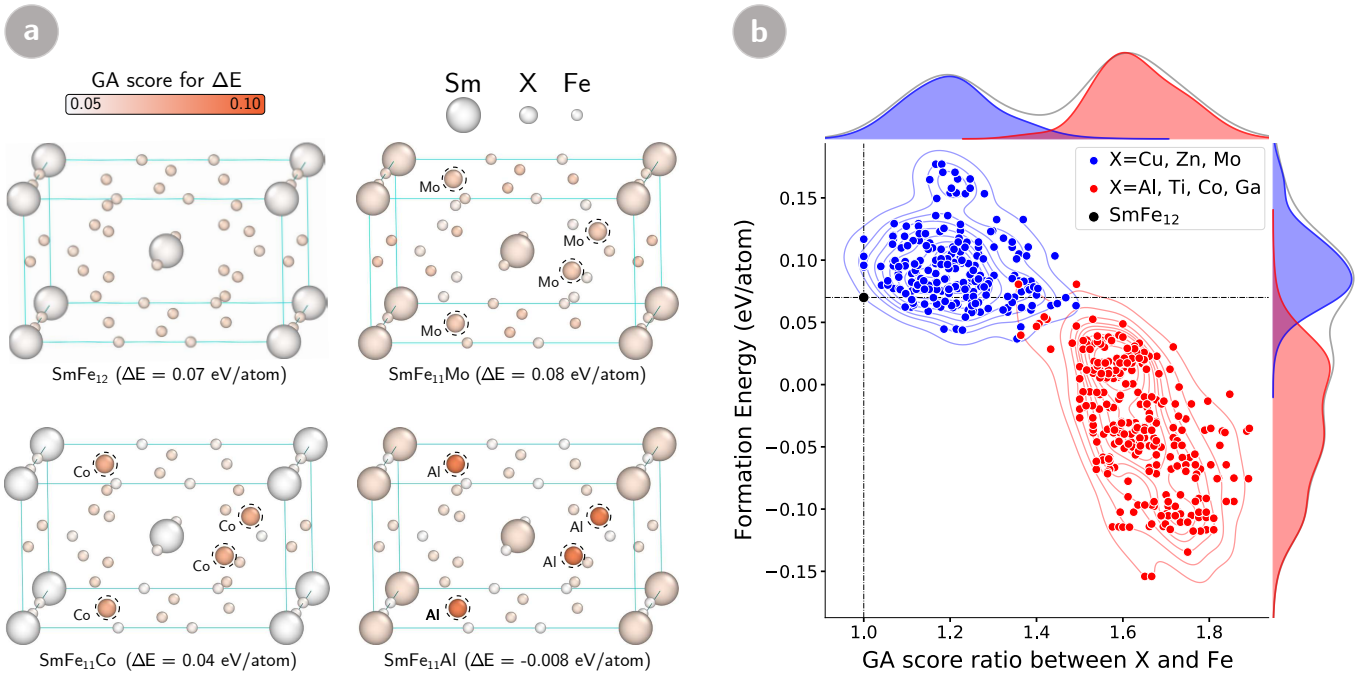

FIG. 7. Visualization of the relationship between structure and formation energy obtained from the SCANNet model for crystalline magnetic materials in $SmFe_{12}$-CD. (a) Visualization of the GA scores estimated by the model for atomic sites in the $SmFe_{12}$, $SmFe_{11}Mo$, $SmFe_{11}Co$, and $SmFe_{11}Al$ crystal structures. (b) Correlation between the ratio of GA scores of the substitution sites to the minimum GA scores among the Fe sites and the formation energy, as calculated via the DFT approach, in crystal structures substituted by a single type of element.

dicate that Mo substitution has little effect on the cage of Fe atoms, whereas the Sm sites become nonnegligible in interpreting the formation energy of the $SmFe_{11}Mo$ crystal structure. This suggests that Sm atoms are less comfortably placed within the Fe and Mo atom cages in the substituted crystal structure. By contrast, for crystal structures substituted with Co or Al, the GA scores of the Co and Al sites are significantly higher than those of Fe sites, indicating that the Co and Al sites should be the central focus of attention when interpreting the formation energy of the $SmFe_{11}Co$ and $SmFe_{11}Al$ crystal structures, respectively. Moreover, the GA scores of Fe sites exhibit a slight decrease, indicating that the Fe atoms become more comfortably placed in the substituted crystal structures.

To validate the interpretation above, the ratio of the GA scores of the substitution sites to the minimum GA scores among the Fe sites is calculated for each crystal structure. Subsequently, the relationship between this ratio and the estimated formation energies of the structures is investigated using DFT calculations. Figure 7b shows that the crystal structures substituted with a single type of element can be divided into two groups: one with Cu, Zn, and Mo substitutions, and the other with Al, Ti, Co, and Ga substitutions. Interestingly, crystal structures with higher local structure GA scores for the substitution sites possess lower formation energies, whereas those with lower local structure GA scores for the substitution sites possess higher formation energies. These results highlight the potential of the SCANNet model in estimating the local structure GA scores for a rational discussion of $SmFe_{12}$-substituted crystal structures and their formation energies. While additional first-principles calculations are necessary for each specific crystal structure to fully understand the relationship between the substitution elements, the substitution sites, and the crystal structure stability, these results confirm the potential usefulness of SCANNet. The local structure GA score provides valuable information and indicate key focus points for understanding the stability of crystalline material structures. Thus, this study offers valuable insights that can contribute to the development of more efficient and effective methods for designing crystal material structures.

III. Discussion

This study proposes an attention-based DL architecture, SCANNet, which leverages attention mechanisms to learn from material datasets, predict material properties, and interpret the underlying features of material structures. By applying attention recursively to neighboring local structures, SCANNet learns representations of atomic local structures in a self-consistent manner. The architecture combines these local structure representations to form a comprehensive representation of the entire material structure, enabling accurate property predictions. During the learning process, global attention

scores are estimated, indicating the importance of each local structure in representing the overall material structure. Experimental results based on four molecular and crystalline material structure datasets demonstrated the excellent predictive capability of SCANNet for different material properties. Furthermore, an in-depth qualitative analysis of the global attention scores of local structures revealed that the trained models can extract essential information from material datasets, facilitating a deeper understanding of the structure–property relationships in both molecular and crystalline materials. This ability of the proposed architecture to interpret the attention scores can aid in identifying critical features and accelerating the material design process.

However, it is important to acknowledge that the interpretability of attention scores in DL models is still a subject of debate and lacks clear guidelines[31–33]. Several factors need to be considered, such as the correlation analysis of attention scores, alternative interpretability metrics, and counterfactual analysis, to validate meaningful explanations of the relationships. Additionally, the quantification and assessment of uncertainty in attention score estimation are essential. Despite these challenges, the findings of this study demonstrate the potential of attention mechanisms in uncovering valuable information that can help in the better understanding of structure–property relationships in materials.

IV. Methods

A. Characterization of material structure

Given a material structure S with the property of interest $y_S \in \mathbb{R}$ containing M atoms ($\mathcal{A}_S = \{a_1, a_2, \cdots, a_M\}$), we consider the structure S as a geometrical arrangement of M local structures. Each local structure consists of a central atom, its neighboring atoms, and their arrangement around the central atom. To determine the neighboring atoms and segment each material structure into local structures, we employ the definition of O'Keeffe[34,35] instead of the assumption about chemical bonds between the atoms in the structure. According to O'Keeffe's definition, all atoms at these atomic sites share Voronoi polyhedron faces with the atomic site of an atom under consideration (the central atom of the local structure) and are regarded as neighboring atoms. Subsequently, the local structures of the neighboring atoms are referred to as the neighboring local structures. Using the information from the Voronoi polyhedron faces, we assess the geometrical influences of neighboring atoms on the central atoms for conveying the structural information of structure S to SCANNet for learning the appropriate representation of S.

For each atom a_i in the structure S, by using the Voronoi tessellation, we can determine $\mathcal{N}_i$ ($\subset \mathcal{A}_S$), which contains N atoms whose atomic sites share Voronoi polyhedron faces with an atomic site of a_i. Subsequently, the geometrical influence of a neighboring atom $a_j (\in \mathcal{N}_i)$ on atom a_i is represented by a vector $\mathbf{g}_{ij} \in \mathbb{R}^h$, which is defined by the element-wise multiplication of the Euclidean distance d_{ij} and Voronoi weight[35] w_{ij} between the atoms as follows:

$$\mathbf{g}_{ij} = \mathrm{DE}(d_{ij}) \times w_{ij} \quad (1 \leq j \neq i \leq M), \tag{4}$$

where $\mathrm{DE}(d_{ij})$ is a distance embedding layer representing the distance d_{ij} as an h-dimensional vector (Supplementary Section II B). As a result, for each atom a_i, we obtain a matrix $\mathbf{G}_{\mathcal{N}_i} = [\mathbf{g}_{ij}]_{a_j \in \mathcal{N}_i}$ representing the geometrical influences of the neighboring atoms of atom a_i. Each row of the matrix consists of a vector $\mathbf{g}_{ij}$ that represents the geometrical influence of atom a_j on atom a_i.

B. Local structure representation

Similar to other DL architectures, SCANNet employs an embedding layer (Supplementary Section II A) to express the atomic information of each atom a_i in S as an h-dimensional vector $\mathbf{c}_i^0$ ($\in \mathbb{R}^h$). Through training, the vector representation $\mathbf{c}_i^0$ is updated and refined to represent the atom more appropriately for accurately predicting property y_S of material structure S.

To learn representations for local structures in material structure S, a local attention layer that utilizes the atomic and geometrical arrangement of atomic sites is proposed. The design of the local attention layer is based on the dot-product key-query attention[16], $\mathrm{Attention}(\mathbf{q}, \mathbf{K}) = \mathrm{softmax}(\mathbf{q}^\top \mathbf{K})\mathbf{K}$, where $\mathbf{q} \in \mathbb{R}^h$ and $\mathbf{K} \in \mathbb{R}^{h \times h}$ denote the query vector and key matrix, respectively. In addition, SCANNet consists of multiple local attention layers to iteratively update the representation of local structures in a layer-wise manner; the $(l+1)^{th}$ local attention layer uses the representations of local structures constructed from the l^{th} layer as inputs. As a result, this design enables SCANNet to efficiently capture information on long-range interaction between local structures in the material structure.

For instance, the representation $\mathbf{c}_i^{l+1}$ ($\in \mathbb{R}^h$) of local structure $\{a_i, \mathcal{N}_i\}$ at the $(l+1)^{th}$ local attention layer is derived from the representation vectors in the preceding layer of itself ($\mathbf{c}_i^l$), its neighboring local structures ($\mathbf{C}_{\mathcal{N}_i}^l = [\mathbf{c}_j^l]_{a_j \in \mathcal{N}_i}$), and the geometrical influence of the neighboring atoms $\mathcal{N}_i$ on atom a_i ($\mathbf{G}_{\mathcal{N}_i}$) as follows:

$$\begin{aligned} \mathbf{c}_i^{l+1} &= \mathrm{LocalAttention}^{l+1}(\mathbf{c}_i^l, \mathbf{C}_{\mathcal{N}_i}^l \times \mathbf{G}_{\mathcal{N}_i}) \\ &= \mathrm{Attention}(\mathbf{q}_i^l, \mathbf{K}_{\mathcal{N}_i}^l) + \mathbf{q}_i^l, \end{aligned} \tag{5}$$

where $\mathbf{q}_i^l = \mathbf{c}_i^l \mathbf{W}_\mathbf{q}^l$ and $\mathbf{K}_{\mathcal{N}_i}^l = (\mathbf{C}_{\mathcal{N}_i}^l \times \mathbf{G}_{\mathcal{N}_i})\mathbf{W}_\mathbf{k}^l$; $\mathbf{W}_\mathbf{k}^l, \mathbf{W}_\mathbf{q}^l \in \mathbb{R}^{h \times h}$ are learnable parameters of the local attention layer and are shared between local structures. The detailed implementation of the local attention layer is described in Supplementary Section II C.

Owing to the application of multiple local attention layers, the attention information regarding a target property between local structures in a material structure S can be passed through the attention relationships between neighboring local structures. In the experiments described herein, a DL architecture including L local attention layers is employed. Consequently, we preserve

the structural information of S from the representations of all its local structures obtained from the final local attention layer, to produce $\mathbf{C}^L$, where $\mathbf{C}^L = [\mathbf{c}_i^L]_{a_i \in \mathcal{A}_S}$.

C. Material structure representation

To represent a material structure S, simple operators, such as the sum or pooling operator, are typically applied to integrate the representations of all local structures in S. However, such operators consider that either the contribution of each local structure to the final structure representation is equal (sum and average-pooling operator)[14,15,25,36] or that the property depends on only the specific local structures in the material structure whereas the others have zero impact (max- and min-pooling operators)[37–39]. Therefore, designing appropriate combination operators for specific target properties is challenging and requires prior hypotheses regarding the structure–property relationships. To overcome this problem, SCANNet again utilizes the dot-product key-query attention[16] to coherently learn the representation of local structures and integrate them into the representation of material structure in a target-dependent manner.

An attention mechanism-based layer, called the global attention layer, is proposed to quantitatively model the attention distribution required across each constituent local structure. This layer aims to obtain a more appropriate representation for the entire structure S. The global attention layer is designed to learn an optimal representation of structure S from data, which subsequently facilitates the construction of a highly accurate predictive model for the target property y_S. The representation vector $\mathbf{x}_S$ of the structure S is formulated by aggregating the representations of all the constituent local structures according to the obtained global attention (GA) scores, as follows:

$$\begin{aligned}\mathbf{x}_S &= \text{GlobalAttention}(\mathbf{C}^L) = \rho(\mathbf{A})\mathbf{K}^g \\ &= \boldsymbol{\alpha}^g \mathbf{K}^g = \sum_{i=1}^{M} \alpha_i^g \mathbf{k}_i^g, \end{aligned} \tag{6}$$

where $\mathbf{A} = \mathbf{Q}^{g\top}\mathbf{K}^g \in \mathbb{R}^{M\times M}$, which $\mathbf{Q}^g = \mathbf{C}^L\mathbf{W}_\mathbf{q}^g$ and $\mathbf{K}^g = \mathbf{C}^L\mathbf{W}_\mathbf{k}^g$ are the query and key matrices, respectively; further, $\mathbf{W}_\mathbf{k}^g, \mathbf{W}_\mathbf{q}^g \in \mathbb{R}^{h\times h}$ are the learnable parameters of the global attention layer. A weighting function $\rho(.)$ is applied to the attention matrix $\mathbf{A}$ to evaluate the GA scores paid to the local structures. As a result, we obtain $\rho(\mathbf{A}) = \text{softmax}([\text{s}_1, \text{s}_2, ..., \text{s}_M])$, in which $\text{s}_j = \sum_{i=1}^{M}[\mathbf{A}(1-\mathbf{I})]_{i,j}$ is the sum of each column j within the attention matrix $\mathbf{A}$ (the identity matrix is denoted as $\mathbf{I}$).

The function $\rho(.)$ is designed based on the assumption that heightened attention should be allocated to local structures whose representations are crucial for accurately representing the other local structures in S. This attention allocation enables the precise prediction of target property y_S. In essence, a local structure that garners higher cumulative attention scores from all the other local structures should be prioritized when representing material structure S. As a result, the degree of attention to a local structure $\{a_i, \mathcal{N}_i\}$ in S is quantitatively modeled by summing all the attention received from other local structures. For a detailed implementation of the global attention layer, please refer to Supplementary Section II D.

Consequently, the physical property y_S of the material structure S can be predicted from the learned representation $\mathbf{x}_S$, as follows:

$$\hat{y}_S = F_S(\mathbf{x}_S), \tag{7}$$

where $F_s : \mathbb{R}^h \to \mathbb{R}^1$ is represented by two fully connected (FC) layers. The weight matrices and bias vectors of the network are learned by training the prediction model.

Furthermore, the GA scores $\boldsymbol{\alpha}^g = [\alpha_1^g, \alpha_2^g, ..., \alpha_M^g]$, which describe the degree of attention given to the corresponding local structures for representing S, are used to reveal critical aspects that help interpret the structure–property relationship of interest. It is important to note that the attention to local structures discussed here signifies the amount of information these local structures contribute to appropriately represent S for accurately predicting y_S.

D. Model training

The training of the DL model using the proposed architecture begins with the initialization of all learnable parameters. All weighting matrices such as $\mathbf{W}_\mathbf{q}^l$, $\mathbf{W}_\mathbf{k}^l$, $\mathbf{W}_\mathbf{q}^g$, and $\mathbf{W}_\mathbf{k}^g$ are initialized to random matrices using Glorot Uniform[40], while the entries of all bias vectors are initialized to zero. The dropout layer and attention dropout[16] are applied in the local attention layers with a rate of 0.1 for better regularization.

In the training process, all parameters of the proposed DL model are updated by minimizing a loss function using *Adam* optimization[41] with a scheduled learning rate decay ranging from 5×10^{-4} to 10^{-4}. To predict the physical property y_S of a material structure S in training dataset $\mathcal{D}$, the loss function is defined as follows:

$$\mathcal{L} = \frac{1}{|\mathcal{D}|}\sum_{S\in\mathcal{D}}(y_S - \hat{y}_S)^2. \tag{8}$$

E. Dataset information

QM9[6]: This computational dataset comprises of data of 133,885 drug-like organic molecules composed of C, H, O, N, and F. However, 3054 files were removed due to the questionable geometric stability[14] that 130,831 molecules remained were used for the experiments. Five physical properties from the QM9 dataset are used as targets for evaluating the predictive capability of the SCANNet models. These properties include the energy of the highest occupied molecular orbital ($\mathbf{E}_{HOMO}$), the energy of the lowest unoccupied molecular orbital ($\mathbf{E}_{LUMO}$), the gap between the energies ($\mathbf{E}_{gap} = \mathbf{E}_{LUMO} - \mathbf{E}_{HOMO}$),

the isotropic polarizability (α), and the heat capacity at 298 K ($\mathbf{C}_v$). In the experiment, the predictive capability of the SCANNet models is compared with that of recent state-of-the-art DL models[14,24–26].

Fullerene-MD[22]: This is an in-house-developed computational material dataset that comprises the data of three well-known fullerene molecules, viz. C_{60} (I_h), C_{70} (D_{5h}), and C_{72} (D_{6h}). It includes optimized structures and 3000 deformed structures obtained from molecular dynamics simulations (1000 structures for each molecule). The HOMO ($\mathbf{E}_{HOMO}$) and LUMO ($\mathbf{E}_{LUMO}$) energies of these structures are determined using DFT calculations, similar to the approach used in the QM9 dataset. Experiments are performed on this dataset to evaluate the predictive capability of the SCANNet models for HOMO and LUMO energies and to assess the interpretability of the models' predictions for these properties. A distinctive feature of all structures in this dataset is that they only contain carbon atoms. Furthermore, due to the symmetric nature of fullerene molecules, the local structures within each molecule are highly similar with only minor differences. Therefore, this dataset allows for a precise evaluation of the interpretability of the SCANNet model. In the evaluation experiment using this dataset, SCANNet models pre-trained on the QM9 dataset are applied to train the prediction models for the HOMO and LUMO energies of the fullerene molecules.

Pt/graphene-MD[22]: This dataset is also an in-house-developed computational material dataset representing a system composed of a platinum atom adsorbed on a graphene flake terminated by hydrogen atoms[42,43]. It consists of data of approximately 21,000 optimized and deformed structures generated through molecular dynamics simulations. The adsorption energies of these structures are determined using DFT calculations, similar to the approach used in the QM9 dataset. The purpose of the experiments conducted on this dataset is twofold: to evaluate the predictive performance of the SCANNet models for deformation energies of the structures (ΔU) and to assess the interpretability of the models' predictions for these deformation energies. The unique structural characteristic of this dataset is the presence of a two-dimensional honeycomb network of carbon atoms forming the graphene flake. Although the local structures of each carbon atom in the system exhibit slight distortions from the ideal sp^2 hybridization structure[43], this dataset allows for the quantitative evaluation of the interpretability of the SCANNet models in terms of the distortion of the honeycomb network on the graphene surface.

$SmFe_{12}$-CD[23]: This dataset is an in-house-developed computational material dataset containing the data of crystalline magnetic materials. It comprises the data of 3307 optimized structures of $SmFe_{12}$-based compounds, along with their corresponding formation energies (ΔE) as the target properties. The dataset was generated by introducing partial substitutions of Mo, Zn, Co, Cu, Ti, Al, and Ga into the iron sites of the original $SmFe_{12}$ structure, which exhibits notable magnetic properties. Subsequently, the structures were optimized, and their formation energies were assessed using DFT calculations. Further details regarding the DFT calculation method used to create this dataset can be found in a previous work[23]. Using this dataset, the predictive capability of the SCANNet models for the formation energies of the structures (ΔE) and the interpretability of the models are quantitatively evaluated to investigate the structural stability of the $SmFe_{12}$-based structures.

Data availability

The in-house-developed computational material datasets related to this article have been deposited to a Zenodo repository[22].

Code availability

The Python implementations for training the SCANNet models and predicting physical properties have been deposited to a GitHub repository[44].

Acknowledgments

This work is supported by the JSPS KAKENHI Grants 20K05301, JP19H05815, 20K05068, and JP23H05403; JST-CREST Program (Innovative Measurement and Analysis), Japan.

Author contributions

T.-S.V., M.-Q.H., D.-N.N., T.T., and H.-C.D. conceived and designed the experiments. T.-S.V., M.-Q.H., V.-C.N., and H.-C.D. performed the experiments. T.-S.V., D.-N.N., H.K., and H.-C.D. analyzed the data. T.-S.V. , D.-N.N., and H.-C.D. contributed materials and analysis tools. T.-S.V., M.-Q.H., and H.-C.D. wrote the paper. T.-S.V., M.-Q.H., D.-N.N., Y.A., T.T., H.T., H.K., T.M., K.T. and H.-C.D. reviewed and edited the paper.

Competing interests

The authors declare no competing interests.

References

[1] A. Agrawal and A. Choudhary, APL Materials **4**, 10.1063/1.4946894 (2016), 053208.
[2] R. Ramprasad, R. Batra, G. Pilania, A. Mannodi-Kanakkithodi, and C. Kim, npj Computational Materials **3**, 54 (2017).
[3] K. T. Butler, D. W. Davies, H. Cartwright, O. Isayev, and A. Walsh, Nature **559**, 547 (2018).
[4] E. M. D. Siriwardane, Y. Zhao, I. Perera, and J. Hu, npj Computational Materials **8**, 164 (2022).
[5] L. Ward and C. Wolverton, Current Opinion in Solid State and Materials Science **21**, 167 (2017).
[6] R. Ramakrishnan, P. O. Dral, M. Rupp, and O. A. Von Lilienfeld, Scientific data **1**, 1 (2014).
[7] L. Himanen, A. Geurts, A. S. Foster, and P. Rinke, Advanced Science **6**, 1900808 (2019).
[8] Y. Zhao, E. M. D. Siriwardane, Z. Wu, N. Fu, M. Al-Fahdi, M. Hu, and J. Hu, npj Computational Materials **9**, 38 (2023).
[9] M. Rupp, A. Tkatchenko, K.-R. Müller, and O. A. Von Lilienfeld, Physical review letters **108**, 058301 (2012).

[10] K. T. Schütt, H. Glawe, F. Brockherde, A. Sanna, K.-R. Müller, and E. K. Gross, Physical Review B **89**, 205118 (2014).

[11] M. Karamad, R. Magar, Y. Shi, S. Siahrostami, I. D. Gates, and A. B. Farimani, Physical Review Materials **4**, 093801 (2020).

[12] T. Xie and J. C. Grossman, Physical review letters **120**, 145301 (2018).

[13] O. Rahaman and A. Gagliardi, Journal of Chemical Information and Modeling (2020).

[14] B. Anderson, T.-S. Hy, and R. Kondor, arXiv preprint arXiv:1906.04015 (2019).

[15] F. B. Fuchs, D. E. Worrall, V. Fischer, and M. Welling, in *Proceedings of the 34th International Conference on Neural Information Processing Systems*, NIPS'20 (Curran Associates Inc., Red Hook, NY, USA, 2020).

[16] A. Vaswani, N. Shazeer, N. Parmar, J. Uszkoreit, L. Jones, A. N. Gomez, L. u. Kaiser, and I. Polosukhin, in *Advances in Neural Information Processing Systems*, Vol. 30, edited by I. Guyon, U. V. Luxburg, S. Bengio, H. Wallach, R. Fergus, S. Vishwanathan, and R. Garnett (Curran Associates, Inc., 2017).

[17] D. K. Duvenaud, D. Maclaurin, J. Iparraguirre, R. Bombarell, T. Hirzel, A. Aspuru-Guzik, and R. P. Adams, in *Advances in Neural Information Processing Systems*, Vol. 28, edited by C. Cortes, N. Lawrence, D. Lee, M. Sugiyama, and R. Garnett (Curran Associates, Inc., 2015).

[18] Z. Wu, B. Ramsundar, E. N. Feinberg, J. Gomes, C. Geniesse, A. S. Pappu, K. Leswing, and V. Pande, Chem. Sci. **9**, 513 (2018).

[19] V. Fung, J. Zhang, E. Juarez, and B. G. Sumpter, npj Computational Materials **7**, 84 (2021).

[20] J. Gilmer, S. S. Schoenholz, P. F. Riley, O. Vinyals, and G. E. Dahl, in *Proceedings of the 34th International Conference on Machine Learning - Volume 70*, ICML'17 (JMLR.org, 2017) p. 1263–1272.

[21] K. Yang, K. Swanson, W. Jin, C. Coley, P. Eiden, H. Gao, A. Guzman-Perez, T. Hopper, B. Kelley, M. Mathea, A. Palmer, V. Settels, T. Jaakkola, K. Jensen, and R. Barzilay, Journal of Chemical Information and Modeling **59**, 3370 (2019).

[22] T.-S. Vu and D. H. Chi, Fullerene structures and Pt absorbed on Graphene structures with HOMO, LUMO and Total energy properties (2023).

[23] D.-N. Nguyen, H. Kino, T. Miyake, and H.-C. Dam, MRS Bulletin 10.1557/s43577-022-00372-9 (2022).

[24] M. Hirn, S. Mallat, and N. Poilvert, Multiscale Modeling & Simulation **15**, 827 (2017).

[25] K. T. Schütt, H. E. Sauceda, P.-J. Kindermans, A. Tkatchenko, and K.-R. Müller, The Journal of Chemical Physics **148**, 241722 (2018).

[26] C. Chen, W. Ye, Y. Zuo, C. Zheng, and S. P. Ong, Chemistry of Materials **31**, 3564 (2019).

[27] F. A. Faber, L. Hutchison, B. Huang, J. Gilmer, S. S. Schoenholz, G. E. Dahl, O. Vinyals, S. Kearnes, P. F. Riley, and O. A. Von Lilienfeld, Journal of chemical theory and computation **13**, 5255 (2017).

[28] T. Ohara, T. Sato, N. Shimizu, G. Prescher, H. Schwind, O. Weiberg, K. Marten, H. Greim, T. D. Shaffer, and P. Nandi, Acrylic acid and derivatives, in *Ullmann's Encyclopedia of Industrial Chemistry* (John Wiley & Sons, Ltd, 2020) pp. 1–21.

[29] U. Schulze-Topphoff, M. Varrin-Doyer, K. Pekarek, C. M. Spencer, A. Shetty, S. A. Sagan, B. A. C. Cree, R. A. Sobel, B. T. Wipke, L. Steinman, R. H. Scannevin, and S. S. Zamvil, Proceedings of the National Academy of Sciences **113**, 4777 (2016).

[30] V. Mantero, L. Abate, P. Basilico, R. Balgera, A. Salmaggi, B. Nourbakhsh, and C. Cordano, Journal of Neurology **268**, 2023 (2021).

[31] S. Jain and B. C. Wallace, CoRR **abs/1902.10186** (2019), 1902.10186.

[32] S. Wiegreffe and Y. Pinter, Attention is not not explanation (2019), arXiv:1908.04626 [cs.CL].

[33] C. Grimsley, E. Mayfield, and J. R.S. Bursten, in *Proceedings of the Twelfth Language Resources and Evaluation Conference* (European Language Resources Association, Marseille, France, 2020) pp. 1780–1790.

[34] M. O'Keeffe, Acta Crystallographica Section A **35**, 772 (1979).

[35] T. L. Pham, H. Kino, K. Terakura, T. Miyake, K. Tsuda, I. Takigawa, and H. C. Dam, Science and technology of advanced materials **18**, 756 (2017).

[36] T.-L. Pham, T.-T. Dang, V.-D. Nguyen, H. Kino, T. Miyake, and H.-C. Dam, Journal of Physics: Conference Series **1290**, 012012 (2019).

[37] Z. Wu, S. Pan, F. Chen, G. Long, C. Zhang, and P. S. Yu, IEEE Transactions on Neural Networks and Learning Systems **32**, 4 (2021).

[38] A. M. Schweidtmann, J. G. Rittig, J. M. Weber, M. Grohe, M. Dahmen, K. Leonhard, and A. Mitsos, arXiv preprint arXiv:2207.13779 (2022).

[39] K. Xu, W. Hu, J. Leskovec, and S. Jegelka, in *7th International Conference on Learning Representations, ICLR 2019, New Orleans, LA, USA, May 6-9, 2019* (OpenReview.net, 2019).

[40] X. Glorot and Y. Bengio, *Proceedings of the Thirteenth International Conference on Artificial Intelligence and Statistics*, Proceedings of Machine Learning Research, **9**, 249 (2010).

[41] D. Kingma and J. Ba, International Conference on Learning Representations (2014).

[42] D. H. Chi, N. T. Cuong, N. A. Tuan, Y.-T. Kim, H. T. Bao, T. Mitani, T. Ozaki, and H. Nagao, Chemical Physics Letters **432**, 213 (2006).

[43] H. C. Dam, N. T. Cuong, A. Sugiyama, T. Ozaki, A. Fujiwara, T. Mitani, and S. Okada, Phys. Rev. B **79**, 115426 (2009).

[44] T. S. Vu, Python implementation of self-consistent atention-based neural network (scannet), `https://github.com/sinhvt3421/scannet-material` (2023).

Supplementary Files

This is a list of supplementary files associated with this preprint. Click to download.

- SupFig1C60.pdf
- Supplement.tex